PIT Project

Behaviour of steel framed structures under fire conditions

STUDIES USING NUMERICAL MODELS : EFFECT OF BOUNDARY RESTRAINTS ON BRITISH STEEL TEST1

Research Report

Report R00-SM3

Abdel Moniem Sanad

The University of Edinburgh
School of Civil & Environmental Engineering
Edinburgh, UK

June, 2000

SUMMARY

The boundary conditions are known to have a major role on the structural behaviour. In order to investigate and evaluate the effect of the boundary conditions assumed in the numerical model developed for British steel first fire test, different boundary conditions were used in parametric studies. In the following paper we describe the finite element model developed for this test and we discuss the effect of the assumed boundary conditions on the behaviour during the test (Paragraph 6). Several studies carried using the same model, also showed that the assumptions used here have very little influence on the model predictions. Those assumptions which are generally based on realistic considerations can be acceptable for the numerical simulations here. A typical example is shown in Figure 15, were two extreme cases of boundary condition (free and fully fixed) are used to study the effect of the boundary condition in the lateral direction outside the fire compartment. The results shown on the figure shows little difference for the two cases. This clearly indicates that the assumption used in the model (full restraint due to the surrounding cold and stiff structure) are acceptable for the simulation.

ABSTRACT

A good engineering assessment of the fire safety of a building structure should be based on a sound understanding of the mechanics of its behaviour under fire. Existing standards and methods of design for fire assume that the structural behaviour is effectively the same as that at ambient temperature, allowing for the reduced material properties. This simple assumption is valid for statically determinate structures, but is in serious error for highly redundant structures, and may be unconservative in certain cases. In particular, the effect of thermal expansion is generally ignored, even though it may swamp the effects of all other phenomena in a large highly redundant building under a local fire.

This paper presents some of the results of an extensive investigation (Usmani *et al.*[14]) in which the structural action in a two-way slab and composite beam structure subjected to a compartment fire has been explored. These results show that thermal expansion dominates the response of highly redundant structures under local fires, and that local yielding and large deflections can be beneficial in reducing damage to the complete structure. However, it is now clear that explicit cognisance should be taken of thermal expansions in design calculations, but this can only be done when a thorough understanding of the behaviour, appropriately generalised, is in place. This is the main motivation behind the results presented in this paper.

INTRODUCTION

Following the Broadgate fire [13], it was clear that the behaviour of real buildings in fire is significantly different from that assumed in current design practice. The full scale fire tests on the BRE multi-storey composite frame at Cardington confirmed this. The Cardington structure was a typical example of current UK steel construction with a concrete profiled deck floor slab acting compositely with hot rolled steel beams, which were mostly left unprotected. The tests showed that very high temperatures could be sustained [7]. However, the test results on their own are insufficient to provide a full explanation of the mechanics that governs the response of such structures to fire. Interactions between thermal expansion, large deformation effects, material degradation and three-dimensional effects in the building lead to complicated behaviour that can only be understood if high quality numerical and analytical models are developed and interrogated. When the effects have been understood, it should be possible to exploit them in design against fire. This paper describes a simple model of the Restrained Beam test to investigate the behaviour an unprotected restrained composite beam during fire.

When a compartment in a large building is exposed to a severe fire, the behaviour of the heated zone is strongly affected by surrounding parts of the structure (outside the compartment) that remain cold, stiff and strong. The interactions between the heated zone, which is expanding and losing strength, and the surrounding cool structure produce several different effects that are difficult to present in the conventional manner, where each member is proportioned as if it were isolated, but subject to stress resultants found from a global analysis. Thus, current practice, based on the behaviour of an isolated element in a test furnace, seriously misrepresents the behaviour of elements of the complete redundant floor system.

Finite element calculations are described that match the experimental observations quite well. These are used to obtain information about quantities that cannot be measured, such as internal forces and moments in a structural element. If the calculation matches the measured responses on those items, which can be measured, then it is reasonable to infer that other parts of the prediction are also realistic components of the complete behaviour. Thus, the calculation of the structure during fire can be used to deduce many features of the response that cannot be deduced in any other way.

Over the last decade many papers have discussed the effect of fire on steel frame structures. One of the first models of the Cardington test frame was by Wang *et al*.[15], which was a 2D model that produced useful conclusions on the critical role of columns. A further theoretical study by Wang [16] indicated the importance of tensile membrane action in maintaining the robustness of composite slabs. Rose *et al.* [8,9] published one of the first 3D models of the Cardington tests, which showed a good match between predicted and test deflections for the Restrained Beam test and the Plane Frame test (Bravery [2]) and the BRE Corner test. However, none of the computational models of the Cardington tests to date have been used to provide a detailed description of the behaviour of the structure, and that is the purpose of this paper.

TEST LAYOUT AND MODEL

The Cardington tests were fully described by Kirby [6]. The Restrained Beam test was designed to study the behaviour of a secondary beam and slab spanning between two columns as shown in Fig. 1. The dimensions of the fire compartment were 8m×3m. The tested beam had a span of 9m, and was connected to a column at each end. The composite profiled deck slab spanned the 3m to the adjacent secondary beams which were supported from the primary beams. The slab was cast in-situ on profiled steel decking (Fig. 4) and had a total thickness of 130mm. The thickness of the steel deck plate was 0.9mm the reinforcement consisted of a single layer of A142 anti-cracking mesh (142 mm^2/m of slab).

Finite element model

The model for the slab was deliberately kept very simple (Sanad *et al.* [12], to simplify the interpretation of the results into images which may be assimilated readily by engineers. For clarity of the descriptions in the rest of this paper, the term ‘joist’ is used to refer to the rolled steel section only, while the term ‘beam’ refers to the composite beam (comprising the steel joist and an appropriate part of the slab). The term ‘longitudinal’ identifies the direction parallel to the secondary joists, whilst the term ‘transverse’ identifies the direction parallel to the primary joists and the ribs formed in the slab by the profiled sheeting (Fig. 1).

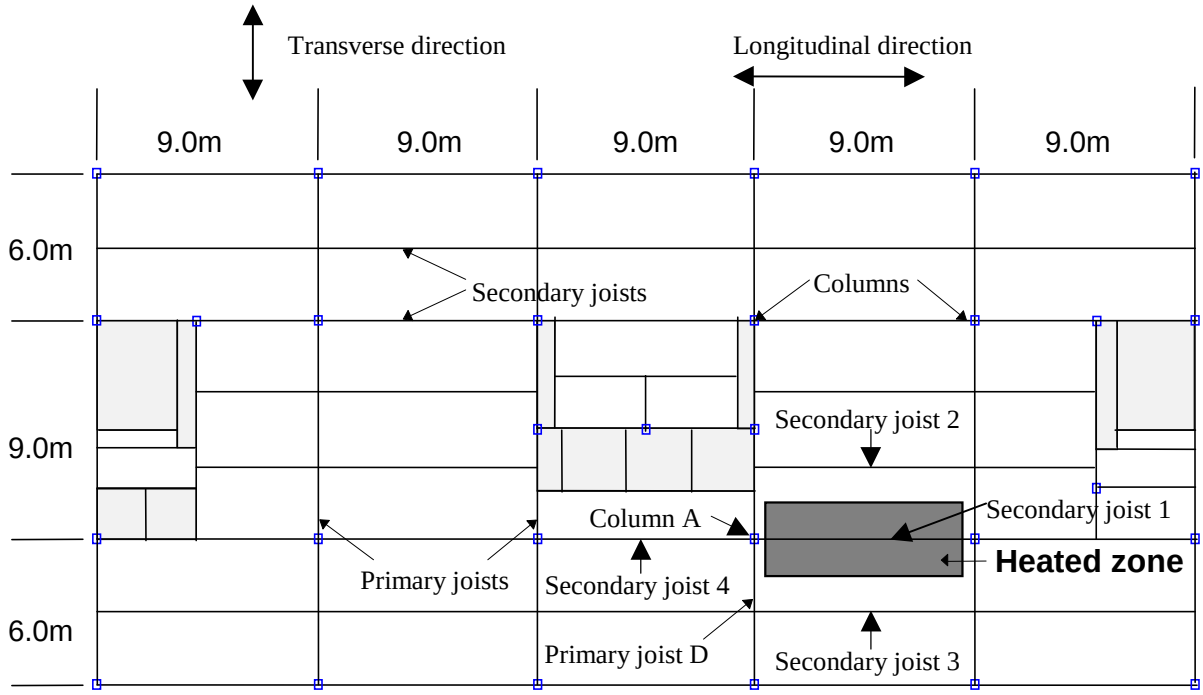

Layout of the Restrained Beam test

Figure 1

The computational model used to simulate the British Steel Restrained Beam test is described here. The finite element model is shown in Fig 2 with the fire compartment area shown shaded. The extent of the model relative to the structure can be deduced by comparing Figures 1 and 2. In the longitudinal (x) direction, symmetry was used at the centre of the compartment and the model included both the column at the end of the beam and the following composite beam to the centre of the adjacent compartment, where symmetry was again assumed. In the transverse (y) direction, the model extended 4.5m on either side of the heated beam to include the adjacent unheated secondary beams and half the span of the next slab. Thus, a total of four secondary joists and two primary joists were used, each treated as a steel thin walled I section rigidly connected to a composite slab. The beam to column connection and beam to beam connections were each modelled with rigid links connecting the displacements and rotations of the beam nodes to those of the column or other beam.

Boundary conditions

At the ends of the ribs the translations in the x & y directions and the rotations about the x & z axes were all restrained (symmetry). All along the primary beam, the x-translation and rotations about the y & z axes were restrained to model the continuity of the slab. At the bottom of the column all displacements and rotations were restrained, whilst at its top only vertical displacement was permitted.

Loading

A distributed load of 5.48kN/m^2, corresponding to the mean dead and live loading of the test was applied directly to the slab ribs. The fire was modelled by heating the slab and the joists up progressively using the measured temperatures of the test until the maximum joist temperature was attained. The temperature measured at the centroid of the slab in the transverse and longitudinal directions and the mid-span temperature of the joist web are shown in Fig. 3, plotted against the time after the start of the fire.

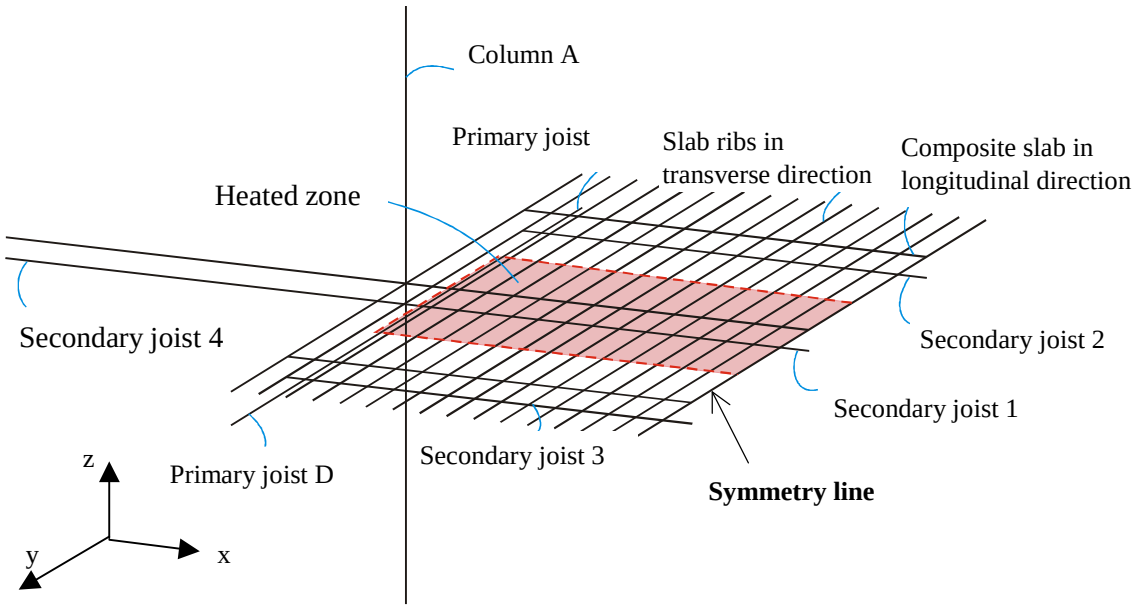

Finite element model for Restrained Beam test

Figure 2

Although the temperature of the different parts of the structure do not increase proportionally with each other, an attempt was made to achieve a model which would not depend so much on the detail of the rate of heating of each part. It was therefore assumed that all temperatures increased linearly from ambient to the maximum value for that member.

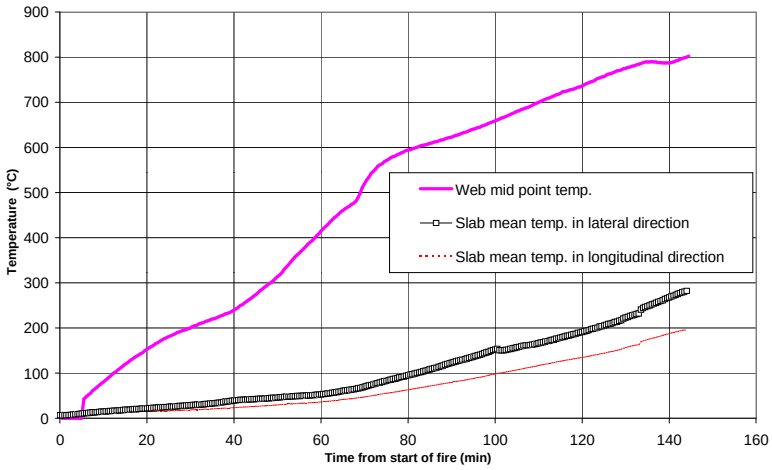

Temperatures in the joist and the slab during the fire

Figure 3

The behaviour of the structure was calculated using a materially and geometrically non-linear analysis, which included thermal expansive strains relating both to the centroidal temperature and the thermal gradient through the depth of each member. The slab temperature distribution was approximated by a linear variation with height, giving an equivalent centroidal value and thermal gradient. These distributions were calculated independently for the longitudinal and the transverse directions.

CONSTITUTIVE MODELLING OF JOIST AND SLAB AT HIGH TEMPERATURE

Section behaviour for hot rolled steel joists

All the steel members were modelled using a standard ABAQUS [1] 2-node thin walled steel I section beam element, with elastic-plastic strain-hardening properties and non-linearly varying temperature-dependent values for all material properties. At ambient temperature strain hardening was included and a yield stress of 300N/mm^2 was used. The variation in temperature through the depth of the section was included, including its effect on both thermal strains and the degradation of material properties at elevated temperatures, based upon ENV [3]. The connections between different steel members were modelled in detail using appropriate constraints on the relative displacements of the nodes associated with each connection.

Slab constitutive model

The orthotropic slab was represented by a grillage because its stiffnesses in the direction of the decking troughs or ribs (transverse) were significantly higher than those in the longitudinal direction. The slab was modelled using a beam member in the transverse direction for the T-beam corresponding to each rib and another beam member above each joist for the composite action of the slab with the joist. This model leads to simple interpretations of composite beam behaviour which can be used to give a clear understanding of the phenomena. In the transverse direction (Fig. 1), the cross-section geometry of slab elements is shown in Fig. 4, and the temperature profile in Fig. 5. A grillage model has obvious limitations: in particular, the in-plane shear stiffness of the slab cannot be modelled accurately and torsional effects are only treated approximately. Despite these limitations, grillage models can capture the key effects, and their interpretation in terms of structural behaviour is much simpler. The results from these models have been compared with a more rigorous approach using an orthotropic plate model (Usmani *et al*. [14]), where the same behaviour was found. Very good quantitative comparisons were obtained on key quantities, such as the axial forces and moments in the composite beam.

The constitutive model for the slab adopted a stress resultant-generalised strain representation. The beam elements had predefined independent force-strain and moment-curvature relationships, determined separately for each direction. This was done using the elastic centroid as the reference axis and calculated using a linear total strain variation through the depth, and non-linear temperature-dependent stress-mechanical strain relationships for the steel and concrete. A special element in ABAQUS [1] (termed ‘beam general section’) permits the user to define the section response in this manner. It was found to produce much more reliable numerical convergence in the calculation at high temperature, where the standard ABAQUS [1] beam and shell elements had caused many numerical difficulties. One disadvantage of using this ‘beam general section’ element was that the interactions between membrane forces and moments could not be included. However, this appears not to have been a major drawback, because the axial forces in the slab are small compared with its ultimate axial force, and the membrane mechanical strains caused by bending are small compared with the thermal strains (and the margin of uncertainty in the thermal strains).

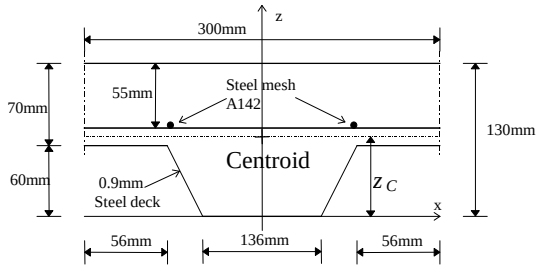

Cross section of the composite slab in the transverse direction

Figure 4

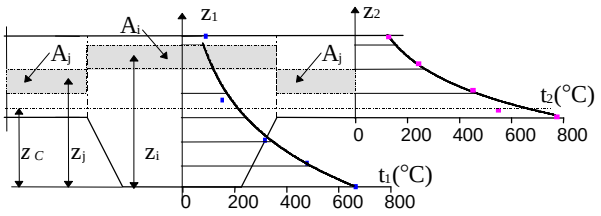

Temperature distributions through the slab depth, and coordinates for integration

Figure 5

Section behaviour for the reinforced concrete slab in the transverse direction

Slab model in each direction

For the transverse direction, the slab was modelled as a series of T-beams corresponding to each rib (Figure 4), with a temperature profile as shown in Figure 5. In the longitudinal direction, the presence of the downstand ribs was ignored, and the whole slab treated as if only the thinner part were present, effectively placing a gap between the top flange of the secondary beam steel joist and the bottom of the slab.

Temperature profile and stress-strain relationships

In the test, the temperature was measured at several points through the slab depth at 4 locations (Fig. 5), some through the thick section of the slab (130mm) and others through the thin section (70mm). Typical temperature distributions through the slab at the end of the fire are shown in Fig. 5. Here, the temperature distribution *T(z)* through the slab at any instant during the fire was approximated by a third degree polynomial with height *z*, with separate assessments for the thick and thin parts. At each instant at each level, the temperature was then taken as known, so the thermal expansion strain and the stress-strain relationship for both steel and concrete were known.

The stress-strain relationships for concrete were adopted from Eurocode 2 (ENV [3]) using an ambient temperature concrete strength of 48MPa, whilst those for steel were taken from Eurocode 3 (ENV [4]) using an ambient yield stress of 280MPa for decking steel and an ambient maximum stress of 700MPa for reinforcement. For concrete experiencing tensile mechanical strains, full cracking was assumed with zero stress.

Axial force - axial strain relationship

For a given temperature profile, the relationship between the axial (or membrane) force and the corresponding centroidal (or membrane) strain in the reinforced concrete slab was approximated in a multi-segment piecewise-linear manner, covering the full range of tensile and compressive strains.

The total strain ε_{ty} at any level z is given by

$$\varepsilon_{ty} = \varepsilon_{tm} + (z - z_C)\phi_t \qquad [1]$$

where z_C is the vertical coordinate of the centroid

ε_{tz} is the total strain at vertical coordinate z

ε_{tm} is the total membrane strain at the section

ϕ_t is the total curvature at the section

Here, the behaviour of the slab is treated as uncoupled between the membrane strain and curvature, so the curvature in Eq. 1 may be taken as zero, and the total strain at all levels is identical to the total strain at the centroid. The total strain at any level ε_{tz} at any instant is next divided into its thermal ε_{Tz} and mechanical ε_{Mz} components giving

$$\varepsilon_{My} = \varepsilon_{tz} - \varepsilon_{Tz} \qquad [2]$$

The axial force F acting on the section (tensile positive) at the membrane total strain ε_{tm} is given by

$$F = \int_0^d \sigma_C(z)\, b(z)\, \mathrm{d}z + \int_0^{d_{SD}} \sigma_{SD}(z)\, b_{SD}(z)\, \mathrm{d}z + \{\sigma_{SR} - \sigma_C\} A_{SR} \qquad [3]$$

where

$b(z)$ is the width of the concrete section at height z

$b_{SD}(z)$ is the width of the steel decking at height z

d is the total depth of the slab

d_{SD} is the total depth of the decking

$\sigma_C(z)$ is the stress in the concrete at height z associated with a mechanical strain ε_{Mz} at temperature $T(z)$

$\sigma_{SD}(z)$, σ_{SR} are the stresses in the steel deck and the reinforcing mesh respectively associated with the corresponding mechanical strains at the corresponding temperatures

A_{SR} is the area of the reinforcing mesh.

The concrete stress was subtracted from the mesh area to simplify the concrete integration. The origin of vertical coordinates (reference level) was taken as the base of the slab (top surface of the steel joists). The integration was performed numerically, dividing the slab depth into ten layers and taking the temperature and strains at each layer as the mean values. This process was applied in turn to the thick and thin parts of the slab. At time t in the fire, the integral then becomes:

$$F = \sum_{i=1}^{np1} \sigma_{Ci}(\varepsilon_{Mz})A_i + \sum_{j=1}^{np2} \sigma_{Cj}(\varepsilon_{Mz})A_j + \sum_{k=1}^{np3} \sigma_{SD}(\varepsilon_{Mz})A_{SD} + \{\sigma_{SR}(\varepsilon_{Mz}) - \sigma_C(\varepsilon_{Mz})\}A_{SR} \qquad [4]$$

where

np1 and *np2* are the number of layers for the thick and thin part of the concrete section

np3 is the number of layers for the steel deck section

A_i is the area of the concrete layer i in the thick part of the slab

A_j is the area of the concrete layer j in the thin part of the slab

The first and third terms are omitted for the longitudinal direction, where it is assumed that the thin part of the slab controls the behaviour.

This axial force - membrane strain relationship has been defined in terms of the total membrane strain ε_{tm} at the section, but the thermal strain at the centroid ε_{T0} is also known,

so Eq. 2 can be used again to characterise the force simply in terms of the mechanical strain at the centroid ε_{Mm}, making it simpler to present. The result of this integration was simplified into a series of piecewise-linear membrane force-membrane mechanical strain relationships at different temperatures. Those for the transverse direction are shown in Fig. 6.

Moment-curvature relationship

At ambient temperature, the steel mesh and steel decking reinforce the concrete slab and provide moment resistance. In the sagging region, the moment capacity of the section is much enhanced by the steel decking. In bending, the strains at all levels in the slab are again given by Eq. 1, but the restrictions of the ABAQUS [1] element mean that the slab must be treated as uncoupled between the membrane strain and curvature. Thus the membrane strain in Eq. 1 may be taken as zero, and the total strain at each level is simply the product $(z - z_C)\phi_t$. The total strain at any level ε_{tz} at any instant is again divided into its thermal ε_{Tz} and mechanical ε_{Mz} components as defined by Eq. 2. The bending moment M about the section centroid (sagging positive) at the total curvature ϕ_t may then be found as

$$M = \int_0^d \sigma_C(z)\, b(z)\, (z - z_C)\, dz + \int_0^{d_{SD}} \sigma_{SD}(z)\, b_{SD}(z)\, (z - z_C)\, dz + \{\sigma_{SR} - \sigma_C\}(z_{SR} - z_C)\, A_{SR} \qquad [5]$$

where z_{SR} is the vertical coordinate of the reinforcing mesh respectively.

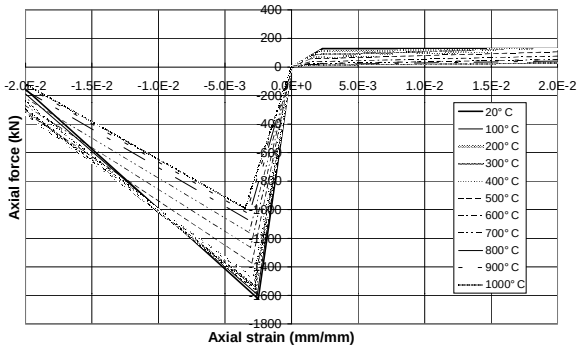

Axial force – axial strain relationship at high temperature in the transverse direction

Figure 6

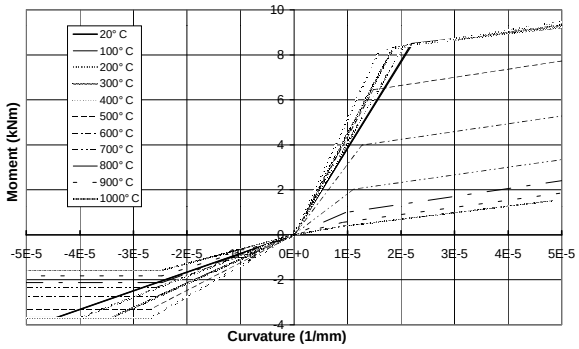

Moment-curvature relationship at high temperature in the transverse direction

Figure 7

Again performing the integration numerically for a wide range of curvatures in both directions, the transverse direction section moment was calculated as

$$M = \sum_{i=1}^{np1} \sigma_{Ci}(\phi_t) A_i (z - z_C) + \sum_{j=1}^{np2} \sigma_{Cj}(\phi_t) A_j (z - z_C) + \sum_{k=1}^{np3} \sigma_{SD}(\phi_t) A_{SD} (z_{SD} - z_C) + \{\sigma_{SR}(\phi_t) - \sigma_C(\phi_t)\} A_{SR} (z_{SR} - z_C) \qquad [6]$$

The first and third terms are again omitted for the longitudinal direction.

Figure 7 shows the resulting moment-curvature relationships in the transverse direction at different temperatures, using the steel decking temperature as reference. The temperature distribution through the slab depth (Fig. 5) indicates that there is a high thermal gradient across the section. When the maximum joist temperature is attained, the top of the slab is

still at a relatively low temperature (below 100°C) whilst the deck steel has reached nearly 700°C. At this temperature, most of the strength of the deck steel is lost, causing the sagging moment capacity to be considerably reduced. In hogging, the section capacity is also somewhat reduced as the reinforcing mesh yield stress drops and the concrete compressive strength declines near the bottom of the slab.

The real slab is a continuous structural plate and its representation by a grillage of beams means that the in-plane shear and torsional stiffnesses are not well modelled. The in-plane bending stiffness and torsional stiffness of each grillage beam was made very high to restrain these freedoms. However this approximation does not appear to be of major consequence in this analysis because the chief structural modes in the slab are out-of-plane bending and in-plane membrane stretching with large deformations.

Composite beam behaviour

The secondary joists were connected into the slab by stud shear connectors, giving the slab the role of the compression flange of a composite beam in the longitudinal direction. It is of course, well known that this composite action develops bending strengths that are far larger than those of the joist or slab alone, but under fire this connection plays a much more important role in connecting the cool slab to the hot joist, transforming its behaviour and susceptibility to fire attack. The shear connectors were modelled here using rigid links: no slip or shear straining of connectors was considered in this model. Similarly the primary joists were connected by stud shear connectors into a composite transverse slab with an effective width of 1.8m.

Section behaviour for composite slab in the longitudinal direction

Axial force - centroidal strain relationship
To achieve a simple model whose behaviour could be understood relatively simply, the slab of the composite beam was assumed to be of constant width along the length of the beam, though it is well known that this width should vary between hogging and sagging regions. For simplicity, the effective width was chosen according to ENV [5], which gave a value of 2250mm based on a slab depth of 70mm. Because the deck steel is corrugated in this direction, it was omitted from the model. The slab cross-section and temperature profile were taken as those of the thinner section, the response calculated using Eq. 3 and simplified into a multi-linear relation (Fig. 8).

Moment-curvature relationships
The bending moments developing within the slab of the composite beam in the longitudinal direction are generally small, so the model is less important. However, the restrictions of the ABAQUS [1] 'beam general section' element meant that a very simple treatment was needed. In the sagging region, the section was treated as a cracked reinforced concrete section in bending, with tensile stresses developing only in the mesh reinforcement. The slab cross-section and temperature profile were again taken as those of the thinner section and the response calculated using Eq. 6, simplified into a multi-linear relation which varied with temperature (Fig. 9).

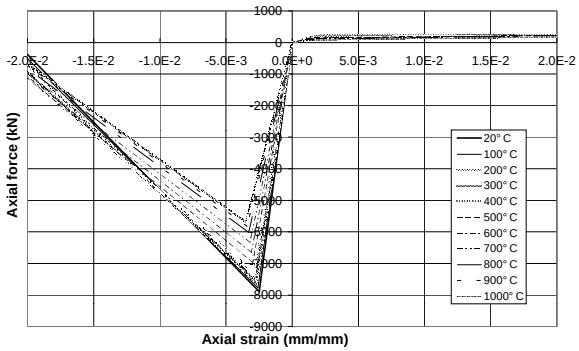

Axial force – axial strain relationship at high temperature in the longitudinal direction

Figure 8

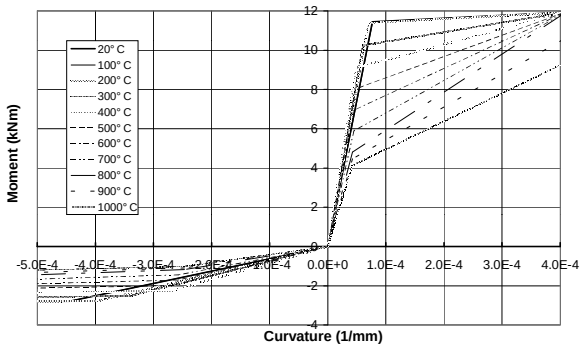

Moment-curvature relationship at high temperature in the longitudinal direction

Figure 9

COMPARISON OF MODEL RESULTS WITH TEST DATA

Some predictions from the numerical model are first compared with experimental observations of three different parameters to show that this simple model does provide a useful prediction of the structural behaviour under fire and to provide some assessment of its accuracy. The quantities compared are the deflection of the joist in the heated compartment at two locations, the horizontal displacement of the column at the level of the connection and strains measured in the unheated Secondary Joist 4 (Fig. 2).

Deflections of the joist in the heated compartment

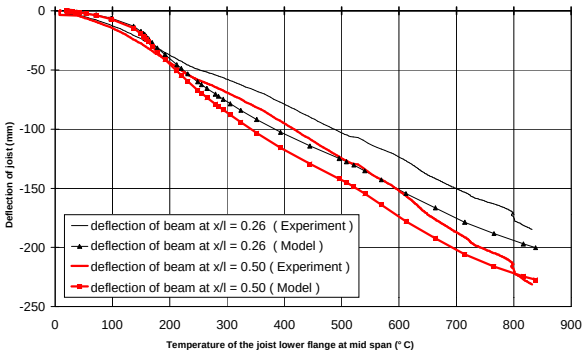

Deflection of the tested joist

Figure 10

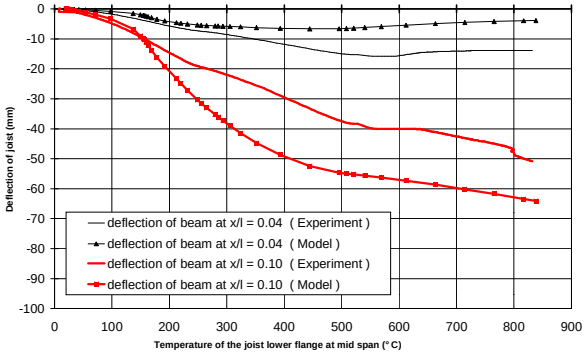

Deflection of the tested joist near column

Figure 11

The test measurements and calculated deflections at two points in the heated secondary joist are shown in Fig.10. Both points were taken on the bottom flange: the first at mid-span and the second at 2.4m from the column. The deflections are plotted against the reference temperature (temperature of the bottom flange at mid-span).

At mid-span, the observed deflection reached a final value of 230mm at 850°C, and the model reproduced this quite accurately, with a maximum difference of about 25mm around 400°C. At one quarter span, the maximum difference between the model and the experiment is also 25mm at about 400°C. There are several reasons for the differences between the computational and test results, which include the simplifications adopted in the model, but the factor that provides the greatest changes in these predicted deflections is the assumed temperature distribution and its evolution with time. It is therefore relatively simple to

change the predicted deflections by modifying the assumed temperature distributions. However, relatively few temperature measurements were made in the slab (only 4 locations over the entire heated zone), and these were insufficient to give a complete spatial distribution, so these predicted deflections do not provide a very good test for the validity of the model. In the predictions shown here, a simple single average of the slab temperatures in each of the thin and thick sections was assumed, though it cannot be known whether this is a good representation of the experiment.

The deflections at two other points on the bottom flange of the heated joist are shown in Fig.11, one at 0.9m and the other at 0.3m from the column centreline (the latter was outside the compartment). Despite the obvious limitations of models of this kind near a restrained point and near the boundary of the compartment, the predicted deflection in each position is comparable to the experimental value.

Horizontal displacement of column

The relative displacement of columns on either side of the tested secondary joist was measured in the test, and due to the symmetry assumed in the model this relative displacement was divided by two to give a measure of the actual horizontal displacement of one column. This value is compared with the numerical predictions in Fig. 12, where there is good qualitative and reasonable quantitative agreement between the model and test results.

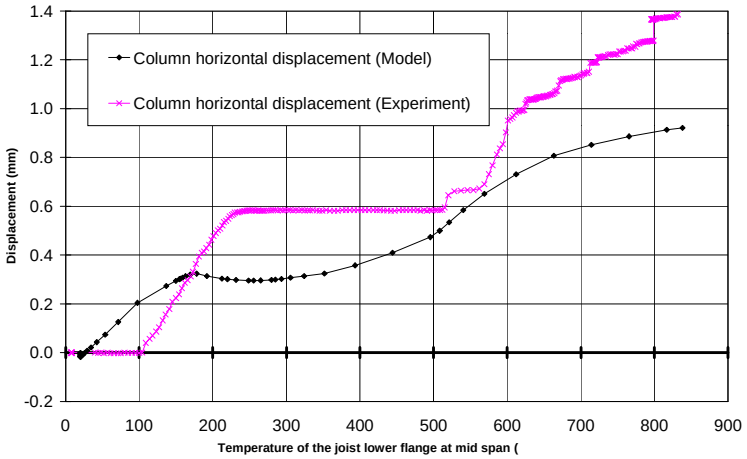

Column displacement at the floor level

Figure 12

This comparison is a very significant because it is strongly related to the overall expansion of the composite beam, which is partly restrained by the cooler surrounding structure. The size of the column horizontal displacements observed in the test suggest that a considerable force was applied by the expanding composite beam against the very stiff cold floor system. The presence of the same pattern of column displacements in the model gives some confidence in the predictions. The variation with time is also significant: rising displacements early in the test corresponds to the heating and expanding of the steel joist. The plateau at moderate temperatures corresponds to the joist reaching its axial resistance (Fig. 16). The later increase in displacement is associated with the expanding slab, which is now considerably hotter. These phenomena can be understood in terms of the development of axial thrust in the composite beam (Fig. 18). Although the magnitude of this displacement is underestimated

probably because the symmetry assumption at the midspan of Secondary Joist 4 overestimates the axial stiffness by about a factor of two, the overall pattern is remarkably similar between the model and test results. Indeed, it is the experimental response that is difficult to explain, where nothing occurred before 100°C, followed by a series of abrupt changes of behaviour: first rapidly rising displacements, then stationary values, then a rapid rise again. No similar comparison to that presented here appears to have been reported in the literature.

Strains over the cross section

Strains were measured on the web and flanges of Secondary Joist 4 on the other side of the column from the heated compartment (see Fig. 2) at 300mm from the connection. The measured values and those predicted by the calculation on the top flange and at the centroid are compared respectively in Figs 13 and 14. These comparisons provide another measure related to the internal forces that develop in the heated composite beam and applied by it to the rest of the structure. The pattern of strain development has three time zones, as was seen with the column displacement, but there is one marked difference: a marked decrease occurs in the strain between 600°C and 800°C, whilst the column displacement rose. This difference arises because the column displacements at high temperatures are driven by the expanding slab, whilst the strain measurements in the steel are dominated by the reduced force the heated joist can develop above 500°C (see also Fig. 17).

At ambient temperature, the calculation indicates a small tensile strain in the top flange (Fig. 13) but the test shows a small compressive strain. The beam is subjected to a hogging moment in this region, and due to the composite action, the slab should be in tension and the joist in compression with the neutral axis in the slab if tensile stresses are sustained by the concrete.

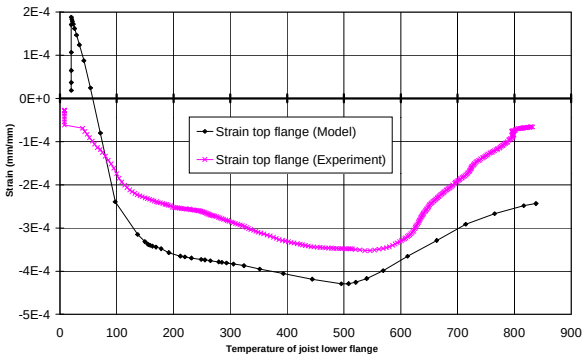

Top flange strain at end of Joist 4

Figure 13

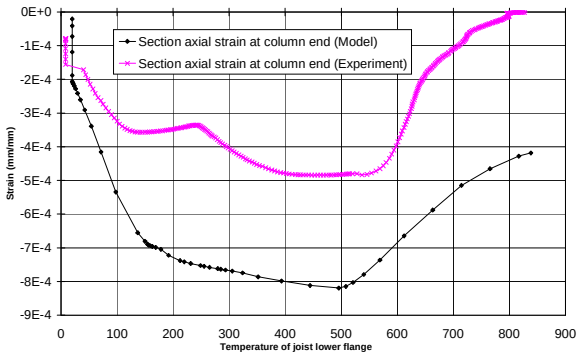

Mean strain at end of Joist 4

Figure 14

In the computer model, a fully cracked approach was used, and the tension stiffening behaviour of cracked concrete was ignored. As a result, the neutral axis at ambient temperature was assessed as lower than the real position, leading to a prediction of tensile strains in the joist top flange. Whilst this simple model underestimates the tensile force carried by a cracked slab at ambient temperature, the error rapidly disappears as the temperature rises and open cracks are closed by thrusts transmitted from the heated beam which is in compression due to restrained thermal expansion.

The calculation again follows the test measurements moderately well over the full range of temperatures. The compressive strain is over-estimated at the joist centroid, where a maximum strain of almost 0.0008 was predicted, though the test only reached 0.0005. This difference is again caused by the use of a symmetry boundary condition at midspan of the Secondary Joist 4, roughly doubling the real stiffness of this axial restraint.

Model sensitivity

Some critical data needed for the calculations cannot be known with any certainty. Two examples are the temperature distribution at points in the slab distant from the thermocouples and assumptions concerning the lateral restraint offered by the surrounding structure. One useful method of testing the significance of such assumptions is to perform two calculations: the first with a simple assumption and a second with a very different and more sophisticated evaluation, but keeping all other data unchanged. If the two calculations lead to very similar results, then it can generally be supposed that there is no need for a complicated model of that particular aspect (there are circumstances where the outcome is, only by chance little affected, but these occasions are rare). Thus a crude model which requires less computer power and less onerous data evaluation can be adopted for further investigations. By contrast, where these comparative calculations show a significant sensitivity to the investigated parameter, it is clear that a crude model will prove unsatisfactory, and the best quality modelling of this parameter must be adopted within any calculation which is to be regarded as reliable. In this study, sensitivity calculations of this kind were performed on many different aspects of the Restrained Beam test.

The effect of the transverse boundary condition on the model behaviour is used here as an example. In the model, the slab ribs were assumed to be fully restrained against lateral translation at their ends. To study the effect of the above assumption, a second calculation was performed where there was no lateral translational restraint at the end of the ribs. The deflection at mid-span in the two calculations is shown in Fig. 15 where the difference in the deflections peaks at only 35mm at 400°C, and is only 10mm at the end of the fire. The relatively small difference between the predictions from two extreme cases for the boundary condition indicates that the deflections predicted by the model have a low sensitivity to the restraint condition at the ends of the transverse ribs. The real restraint condition, associated with a cold and stiff surrounding slab, is likely to be similar to a rigid restraint, especially when the properties within the compartment decline at high temperature. Thus, the assumption adopted in this model is not unreasonable. It may also be noted that the ends of these ribs are quite distant from the tested joist. The cold composite slab above the adjacent secondary Joists 2 and 3 (see Fig. 2) provides considerable restraint for the development of compressive membrane forces as well as anchorage for tensile membrane forces in the ribs.

Similar investigations were made to check the sensitivity of the model to assumptions about temperature distributions (gradients and centroidal temperatures), connection modelling, local buckling of heated joist and joist section sizes (see Usmani *et. al.* [14]).

STRUCTURAL BEHAVIOUR DURING FIRE

The main purpose in developing the numerical model described above was to provide an understanding of the behaviour of the structure and the different phenomena occurring during the entire heating period of the fire. An analysis of the internal forces that develop in the

structure provides an adequate understanding of the local and global behaviour. A description of the structural behaviour seen within the calculation is given below. Wherever possible, the deductions are related to experimental observations.

Behaviour of the steel joist near the connection to the column

Axial thrusts develop in the heated Secondary Joist 1 during the fire. The value near the column is plotted in Fig. 16 against the reference temperature of the joist lower flange at mid-span. The fully plastic axial force capacity Af_y of the joist at each temperature is shown for comparison, though the presence of bending in the joist means that these values should not be attainable. The maximum attainable axial force, including all strain hardening, is also shown, though this could only be reached with huge strains.

At ambient temperature. the joist is in compression due to the hogging moment in the composite section at the column end. Restrained thermal expansion causes a rapid rise in the compression force as soon as heating begins. At 150°C (Point A in Fig. 16), the axial force in the section reaches the fully plastic axial force capacity Af_y and thereafter extensive plastic straining with strain hardening occurs in the joist.

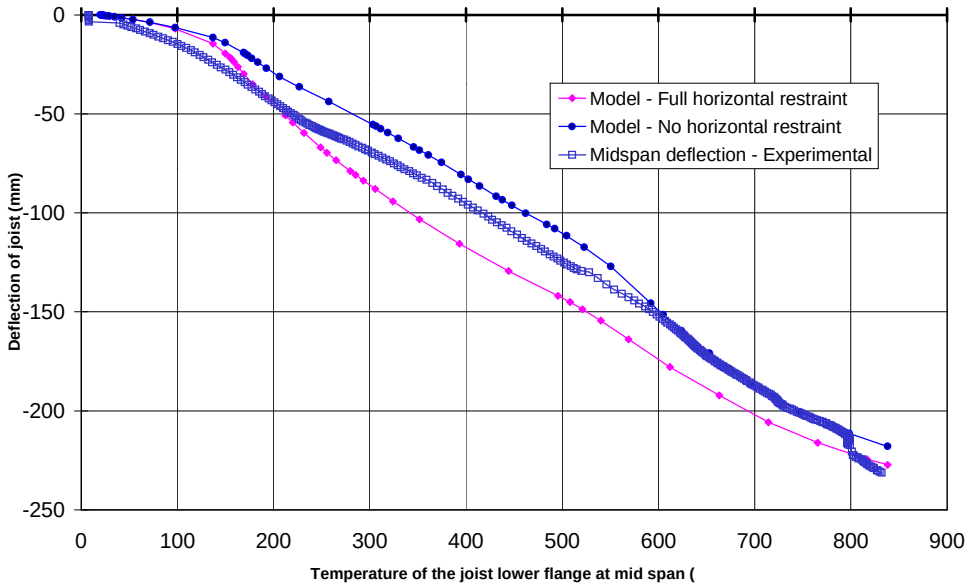

Deflection at mid-span using different assumed rib end boundary conditions

Figure 15

The section capacity does not decline with the reference temperature because this point is outside the compartment and the final temperature reached here was only 220°C. A second event occurs at 500°C (Point B in Fig. 17), but the reason for this is to be found later.

Behaviour of the steel joist just inside the heated compartment

The axial thrusts just inside the compartment (0.9m from the column) is plotted in Fig. 17, together with the fully plastic axial force and first yield axial force relevant to the local temperature. The first yield axial force has little significance at high temperature (Fig. 17), simply marking the beginning of nonlinearity. The evolution of thrust is similar to that at the adjacent section near the column, with a rapid increase in thrust due to restrained thermal

expansion at low temperatures. Between Points A and B the thrust is limited by equilibrium and the events shown in Fig. 16. However, at 500°C (Point B) the thrust in the joist approaches the full plastic yield surface, and from here on until the end of the fire, the thrust is limited by material degradation inside the compartment. This is the reason why the thrust in Fig. 16 also declines. This event (B) in the model matches the test observation of plastic buckling of the web at this location at approximately 500°C.

Thus, although bending causes larger axial thrusts near the column than within the compartment, the ultimate capacity of the joist there is scarcely changed during the fire, and it is the point just within the compartment that limits the development of thrust at very high temperatures.

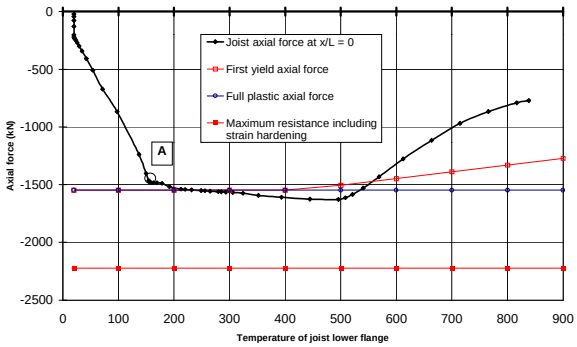

Joist axial force at column

Figure 16

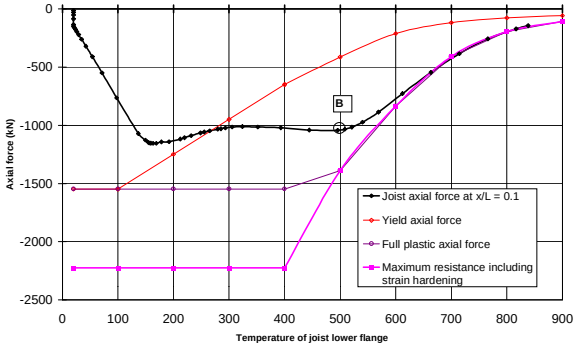

Joist axial force at compartment boundary

Figure 17

Behaviour of the composite beam

The axial forces developing in the complete composite beam at the column and at mid-span are shown in Fig. 18, where the coincidence of the curves shows that each section in this grillage model is subject to the same compressive force. The shape of the curve shows the rapid (linear) development of thrust due to restrained thermal expansion up to 150°C. From 150°C to 500°C, a further rise is seen caused by restrained expansion of the concrete slab where considerable compressive forces develop (cf Fig. 16). Beyond 500°C, the total thrust declines, driven by the degrading steel thrust (Fig. 17), but partly offset by further increase in slab compression. Thus the total thrust in the composite member is controlled by the local degradation of the joist. The two abrupt changes at Points A and B are caused by the events described above.

The increasing thrust developed in the composite beam (Fig. 18) combined with its deflection (Fig. 10) causes a P-Δ moment (Fig. 19). This P-Δ sagging moment develops slowly whilst the deflections are small (to Point A), but then grows fast under a relatively constant thrust but with linearly increasing deflections, and by 300°C it exceeds the moment due to the applied load (Figure 19). In addition to these P-Δ moments, the difference between the temperatures of the steel and concrete constitute a thermal gradient in the composite beam that causes a hogging moment to develop over its entire length (Rotter *et al* [10,11], Usmani *et al*. [14]).

Both the P-Δ moment and the hogging thermal gradient moment can be described as thermally induced stress resultants that affect the behaviour strongly. The moments in the

composite beam at the support and at mid-span are shown in Fig. 20. At ambient temperature, the classic composite beam pattern of sagging at mid-span with a smaller hogging moment at the end occurs. As the temperature rises to 150°C, the thermal gradient hogging moment develops strongly until the beam is almost entirely under a hogging moment. At 150°C the end of the joist reaches axial yield and the hogging capacity stabilises. The moment at mid-span then increases, with increasing thrust developing in the slab, until 300°C when it is rather stable until 500°C. From 550°C to the end of the fire, the moment at each of the two sections reduces due to the reducing properties of the joist.

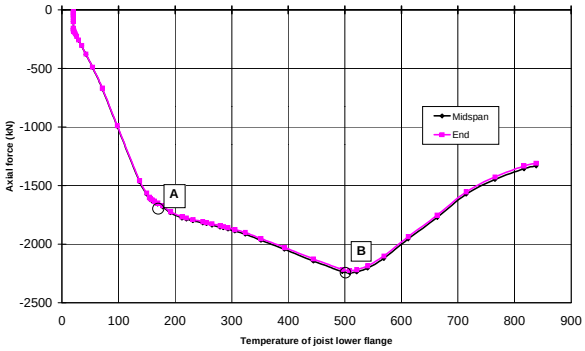

Composite axial force during fire

Figure 18

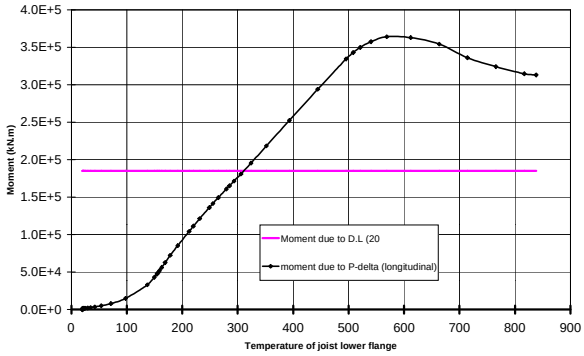

P-Δ moment at mid-span

Figure 19

If the beam is considered as a single structural element, the difference between the moment at the end and at mid-span represents the total moments due to external forces on the beam. Here, it is a combination of forces due to dead and live loads transferred from the slab ribs, together with P-Δ moments. This total moment is the upper curve in Figure 21. At 20°C, the total moment corresponds to the free bending moment diagram due only to the applied loads. The value remains relatively constant up to 150°C because the slab is very cool at this stage. However, as the slab expands, the composite beam capacity rises, and the beam is able to carry increased total moments up to 300°C, sustaining them until 500°C, but then slowly reducing in capacity as the steel weakens to the end of the fire. The thrust developing in the slab due to restrained thermal expansion thus has a very beneficial effect on the flexural capacity of the composite beam, in a similar manner to pre-stressing.

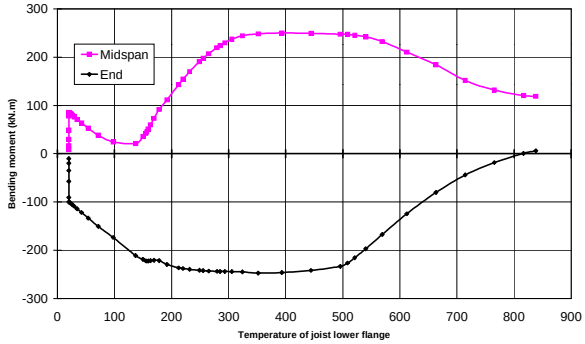

Composite moment at support and mid-span

Figure 20

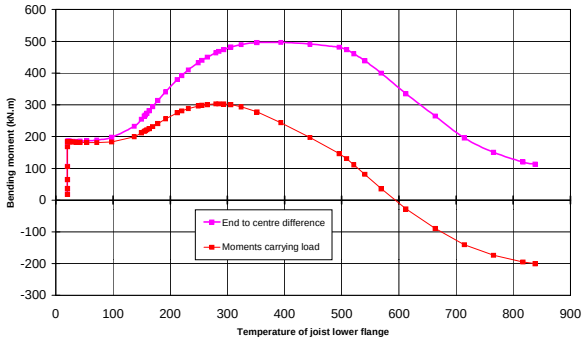

Moments over the composite beam

Figure 21

The lower curve on the same figure shows the net moment attributable to external loads on the beam (total moment minus the P-Δ moment), which indicates the contribution of this heated composite beam to the total equilibrium of the floor system (a positive sign indicates

that the beam is carrying loads; a negative sign indicates that the beam is applying loads to the rest of the structure). It is clear from Fig. 21 that the composite beam imposes a load on the rest of the structure from 550°C until the end of the fire. The ribs of the transverse slab then provide membrane action to support the load capacity of the complete floor.

Tensile membrane action

The axial forces developing in the ribs of the slab in the transverse direction are shown in Figure 22. At ambient temperature, these membrane forces are tiny. Between 20°C and 200°C, the ribs develop compressive forces as their expansion is restrained by the cold surrounding slab. The magnitude of the compressive force developed in each rib depends upon its location (Fig. 22) because deflections permit the expansion to be accommodated without compressive force development (Rotter *et. al.*[8]). Thus the ribs near the primary beam develop higher compressions because they deflect less and those near mid-span develop lower compressions because they deflect more. From 200°C onwards the axial compression in every rib reduces, and the ribs near mid-span (x/L=0.4 & x/L=0.5) develop tension at temperatures above 500°C. This corresponds to the period when the composite beam begins to apply additional loading to the transverse slab (Figure 21).

The tensile membrane action is mobilised by the large displacement effects as the relative magnitudes of joist deflections and rib thermal expansion compete under the requirements of compatibility. It should be noted that quite small tensile forces can carry substantial loads because the deflections have already become large, and these tensile forces in slab lie far below its tensile capacity at the relevant elevated temperatures.

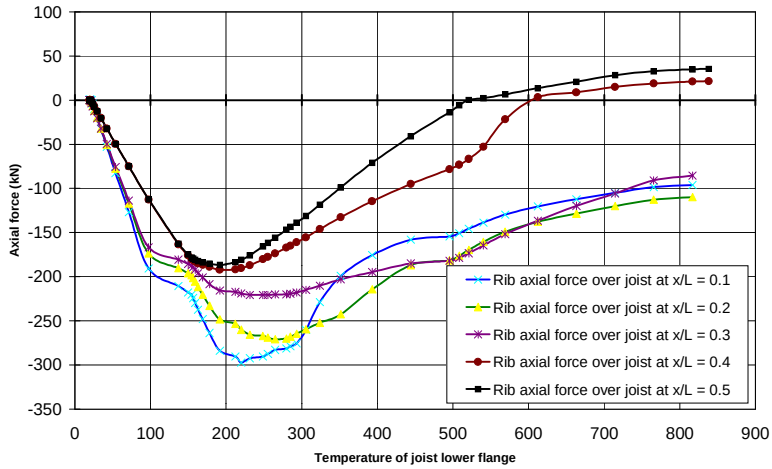

Membrane forces in the transverse direction in the slab (ribs)

Figure 22

CONCLUSIONS

A relatively simple numerical model has been presented in this paper and applied to the analysis of the Cardington Restrained Beam test. Some of the advantages of this simple model have been exploited to deliver a clear image of the structural behaviour within the 3D building, which can be used with later more complicated models as a template for interpreting them.

Several quantitative comparisons have been made with different parameters observed in the test, showing a relatively good agreement, and far exceeding any known previous verification. The numerical results have been interrogated in some detail to allow a comprehensive picture of structural behaviour to be derived. The results presented here have now been confirmed using more sophisticated models that represent the slab using shell elements (Usmani *et. al.* [14]).

The paper has shown the patterns of the development of forces and moments within the building structure, and explained why the building was able to support its loads at temperatures far in excess of those at which runaway failures might occur in determinate structures. The results confirm that it is the thermal effects of restrained expansion and bowing due to vertical thermal gradients that govern the response of the structure for the whole temperature range of the fire. The internal forces developed in the structure far exceed those caused by the imposed loads. The analysis has also shown that, despite being subjected to enormous thermally imposed loads and the loss of steel strength, the continuity of the slab system provides robust redistribution paths to maintain structural stability. In particular, the prestressing effect of restrained thermal expansion of the slab permits large deflections to develop before material degradation becomes overwhelming, and thus allows large deflection load carrying mechanisms to form well within the strength and deformation limits of the slab structure.

REFERENCES

[1] ABAQUS (1994) "ABAQUS theory manual and users manual", Version 5.4, Hibbit, Karlsson and Sorensen Inc., Pawtucket, Rhode Island, USA.

[2] Bravery, P.N.R. (1993) "Cardington large building test facility: construction details for the first building", Internal report British Steel plc.

[3] ENV 1992-1-2 (1995) "Design of concrete structures, Part 1.2: General rules- Structural fire design", Eurocode 2 Part 1.2.

[4] ENV 1994-1-1 (1994) "Design of composite steel and concrete structures, Part 1.1: General rules and rules for buildings", Eurocode 4 Part 1.1.

[5] ENV 1993-1-2 (1995) "Design of steel structures, Part 1.2: Fire resistance", Eurocode 3 Part 1.2.

[6] Kirby, B.R. (1997) "Large scale fire tests: the British Steel European Collaborative Research Programme on the BRE 8-Storey Frame", Fifth International Symposium on Fire Safety Science, Melbourne, Australia.

[7] O'Connor M.A. and Martin D.M. (1998) "Behaviour of a multi-storey steel framed building subjected to fire attack", *Journal of Constructional Steel Research*, 46: 1-3.

[8] Rose P.S., Bailey C.G., Burgess I.W. and Plank R.J. (1997) "The influence of floor slabs on the structural performance of the Cardington frame in fire", in Structures in the New Millenium, Balkema, Rotterdam.

[9] Rose P.S., Burgess I.W., Plank R.J. and Bailey C.G. (1998) “The influence of floor slabs on the structural behaviour of composite frames in fire”, Journal of Constructional Steel Research, Vol. 46, Nos 1-3.

[10] Rotter J.M., Sanad A.M., Usmani A.S. and Gillie M. (1999) “Structural performance of redundant structures under local fires”, Proceedings of Interflam’99, Interscience Communications Ltd. London, No.2-1999, 1069-1080.

[11] Rotter, J.M. (1999) “Behaviour of highly redundant buildings under compartment fires”, Invited plenary paper, Proc., International Conference on Structural Steelwork, ICASS’99, Vol. 1, Hong Kong, December 1999, pp. 39-50.

[12] Sanad A.M., Rotter J.M., Usmani A.S. and O’Connor M.A. (1999) “Finite element modelling of fire tests on the Cardington composite building”, Proceedings of Interflam’99, Interscience Communications Ltd. London, No.2-1999, 1045-1056.

[13] Steel Construction Industry Forum, Structural fire engineering (1991) “Investigation of Broadgate Phase 8 fire”, Steel Construction Institute (SCI).

[14] Usmani A.S., O’Connor M.A., Rotter J.M., Elghazouli A.Y., Drysdale D.D., Sanad A.M., Gillie M. and Lamont S. (2000) DETR-PIT Project “Behaviour of Steel Framed Structures under Fire Conditions”, Final Report (*draft*), March (final version June 2000).

[15] Wang Y.C., Lennon T. and Moore D.B. (1995) “The behaviour of steel frames subject to fire”, *Journal of Constructional Steel Research*, 35:291-322.

[16] Wang Y.C. (1996) “Tensile membrane action in slabs and its application to the Cardington fire tests”, Proceedings of the 2nd Cardington Conference, March, BRE.